Macromodeling of Electric Machines From Ab Initio Models

Ajay Pratap Yadav, *Student Member, IEEE*, Tuncay Altun, *Student Member, IEEE*, Ramtin Madani, *Member, IEEE*, and Ali Davoudi, *Senior Member, IEEE*

***Abstract*—We extract the lumped-parameter model of a wound-rotor synchronous machine from its physics-based magnetic-equivalent circuit model. Model extraction is formulated as a weighted least square optimization with nonlinear constraints in which time-domain trajectories of flux linkages, currents, and the electromagnetic torque are used as input data to obtain the parameters of the $qd0$ model of the machine. The resulting problem is non-convex and cannot be solved using standard methods. The optimization problem is, therefore, convexified using a cone programming relaxation. The solution to the relaxed problem is used as an initial point for the interior-point method, leading to a reliable framework. Accurate estimations on stator resistance, leakage and mutual inductances in stator and rotor, rotor speed, effective turns-ratio between the field and stator windings, and the number of poles are obtained. Estimated parameters are validated against measured and estimated values reported in literature, and are used to develop a behavioral $qd0$ macromodel of the machine.**

***Index Terms*—Convex relaxation, magnetic-equivalent circuit, parameter estimation, cone programming, wound-rotor synchronous machine.**

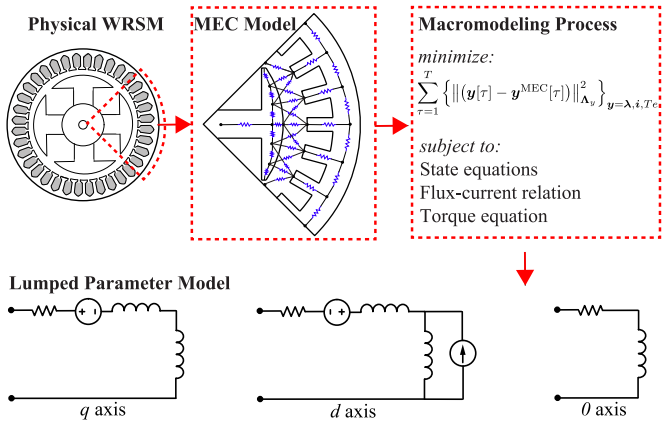

Fig. 1. $qd0$ model extraction from the MEC model of a WRSM.

I. Introduction

ELECTRIC machine models can be classified into lumped-parameter models, such as abc phase-domain models, $qd0$ models, or voltage-behind reactance models [1], and those based on the first principles of physics (Maxwell equations), such as finite-element methods (FEM) or magnetic equivalent circuits (MEC). Lumped-parameter macromodels are suitable for system-level studies, drive-controller design, or hardware-in-the-loop applications [1], [2]. FEM models are highly accurate and closely mimic the hardware, but they are computationally expensive and mainly used for the final design verification. MEC modeling is an intuitive approach based on the circuit theory. Herein, we extract the lumped parameters of a dynamic *qd0* model from the data generated by the MEC model. We use a mesh-based MEC model of a wound-rotor synchronous machine (WRSM) [3]–[6] as it exhibits better numerical properties than its nodal-based counterpart [7]. WRSMs are used in various applications, e.g., aircraft generators, ship propulsion, and wind turbines [8]. $qd0$ model extraction is analogous to replacing the spatially-distributed reluctance network of the MEC model with equivalent lumped-parameter components (see Fig. 1).

IEEE Std-115 [9] documents an array of tests to identify synchronous machine parameters. Since it is not always feasible to run all the necessary tests, various techniques estimate machine parameters using transient measurements [10]–[14]. In the absence of hardware measurement, high-fidelity physics-based models, that closely mimic the experimental prototype, can be used instead. Furthermore, detailed models provide access to a host of variables that might not be available experimentally due to a limited sensory. [15] and [16] have used FEM models to determine the parameters of equivalent circuits for induction machines. [17] has used the data from a pulse test applied to the FEM model of a synchronous machine to obtain its lumped-parameter model. However, MEC models have not yet been exploited for such macromodeling purposes. Another aspect of our contribution is the extraction methodology. While optimization methods based on convex relaxation have found wide applications in power system areas [18]–[20], they have not yet been properly explored for model extraction and parameter estimation of electric machines [21], [22]. We formulate the parameter extraction process as a weighted least-square problem with nonlinear constraints such that it minimizes the mismatch between trajectories produced by the MEC model and those predicted by the $qd0$ model.

Manuscript received July 31, 2019; revised December 17, 2019; accepted January 28, 2020. Date of publication February 3, 2020; date of current version May 20, 2020. This work was supported by the National Science Foundation under Grant ECCS-1509804. The work of T. Altun was supported by the National Science Foundation under Award ECCS-1809454. Paper no. TEC-00803-2019. *(Corresponding author: Ali Davoudi.)*

The authors are with the Department of Electrical Engineering, University of Texas, Arlington, TX 76019 USA (e-mail: ajay.yadav@mavs.uta.edu; tuncay.altun@mavs.uta.edu; ramtin.madani@uta.edu; davoudi@uta.edu).

Color versions of one or more of the figures in this article are available online at http://ieeexplore.ieee.org.

Digital Object Identifier 10.1109/TEC.2020.2970965

Due to the presence of nonlinear equality constraints, the proposed optimization problem is non-convex and cannot be solved reliably using standard interior-point method (IPM) solvers [23]–[25]. To eliminate the need for initialization we propose a hybrid optimization framework based on cone programming relaxation. We relax the original problem and feed the resulting solution to IPM in order to arrive at fully-feasible and globally optimal solutions [26]. The contributions of this paper are summarized below:

- We have recovered machine parameters, namely stator resistance, rotor speed, stator leakage inductance, q-axis magnetizing inductance, d-axis magnetizing inductance, equivalent turns-ratio between the field and the stator windings, and the number of poles. Extracted parameters are compared against those values reported in literature.
- The model extraction is formulated as a non-convex optimization problem using a hybrid cone programming and IPM approach.
- The extracted $qd0$ model is validated against the MEC model, and shown to capture dominant dynamical modes with more than 20 times faster model execution.

The outline of the paper is as follows. Section II is a preliminary review on the symbols and notations used throughout the paper. Section III presents the dynamic MEC model and the target $qd0$ model for WRSM. Section IV elaborates a discrete $qd0$ model for WRSM, and formulates the parameter extraction process as a non-convex optimization problem. Section V presents cone programming relaxation and objective penalization. Section VI studies the implementation process and results. Finally, Section VII concludes the paper.

II. Notation

Matrices and vectors are presented as bold uppercase and lowercase variables, respectively (e.g., $\mathbf{X}$ or $\mathbf{x}$). $\mathbf{x}_i$ denotes the ith element of vector $\mathbf{x}$. $\mathbf{X}_{ij}$ denotes the element in the ith row and jth column of matrix $\mathbf{X}$. $\mathbb{R}^n$ is the set of column vectors of size $n \times 1$. $\mathbb{R}^{m\times n}$ is the set of matrices of size $m \times n$. $\mathbb{S}^n$ denotes the set of symmetric matrices of size n. $\mathbf{0}_m$ and $\mathbf{1}_m$ represent vectors of size $m \times 1$ with all their elements as 0 and 1, respectively. Similarly, $\mathbf{0}_{m\times n}$ represents a matrix of size $m \times n$ with all its element equal to 0. $\boldsymbol{I}_n$ is an identity matrix of size n. $||\mathbf{x}||_2$ denotes the Euclidean norm of the vector $\mathbf{x}$. $\mathrm{diag}(\mathbf{x})$ gives a diagonal matrix with elements of the vector $\mathbf{x}$ along its diagonal. $\mathrm{diag}(\mathbf{X})$ gives a vector with its elements the same as the diagonal of the input matrix. $\mathrm{diag}(\mathbf{X}, \mathbf{Y})$ produces a block diagonal matrix with input matrices along its diagonal. $(\cdot)^\top$ indicates the transpose operation. $||\mathbf{x}||^2_{\mathbf{Z}}$ represents $\mathbf{x}^\top\mathbf{Z}\mathbf{x}$. $\langle \mathbf{X}, \mathbf{Y}\rangle$ stands for the inner product of matrices $\mathbf{X}$ and $\mathbf{Y}$. $^-$ denotes the square of a variable, e.g., $\overline{x}$ represents x^2 for a scalar x and $\overline{\mathbf{x}}$ is a vector with elements of $\mathbf{x}$ squared. $\sqrt{\mathbf{x}}$ denotes an element-wise square root operation on vector $\mathbf{x}$.

III. Ab Initio and Lumped-Parameter WRSM Models

A. Dynamic MEC Model

This section presents a concise overview of the mesh-based MEC model of the WRSM in [3]–[6]. We have selected the static MEC model in [3] and formed a dynamic MEC model using the procedure laid out in [6]. Therein, the field current and rotor speed are assumed constant. Damper windings are ignored in [3]–[5]. Different segments of stator, rotor, and airgap are modeled using flux tubes to form a magnetic circuit, as seen in Fig. 1. Reluctance formulation is based on the geometry and permeability information of respective flux tubes [6]. Kirchhoff's voltage law on individual loops gives

$$\overline{\boldsymbol{\mathcal{R}}}\boldsymbol{\Phi} = \boldsymbol{\mathcal{F}}, \tag{1}$$

where $\overline{\boldsymbol{\mathcal{R}}} \in \mathbb{S}^{nl}$ is the matrix of reluctances, $\boldsymbol{\Phi} \in \mathbb{R}^{nl}$ is vector of flux terms in each loop, $\boldsymbol{\mathcal{F}} \in \mathbb{R}^{nl}$ is the vector of MMF sources, and nl is the number of loops. Note that due to the rotor motion, the reluctances of the flux tubes in the airgap region in matrix $\overline{\boldsymbol{\mathcal{R}}}$ changes with time and should be recalculated at every step. The elements of $\boldsymbol{\mathcal{F}}$ can be obtained as the product of winding turns and currents for each magnetic loop. One can get the flux linkages, $\boldsymbol{\lambda}_{abcs}$, using [5]

$$\boldsymbol{\lambda}_{abcs} = P\mathbf{N}^\top_{abcs}\boldsymbol{\Phi}_{st}, \tag{2}$$

where P is the number of poles, $\mathbf{N}_{abcs}$ is the turns matrix for stator windings, and $\boldsymbol{\Phi}_{st}$ represents the flux in loops corresponding to stator segments of magnetic circuit.

[6] has reformulated (1) such that flux linkages, $\boldsymbol{\lambda}_{abcs}$, are the inputs and winding currents, $\boldsymbol{i}_{abcs}$, are the output.

$$\begin{bmatrix} \overline{\boldsymbol{\mathcal{R}}} & -c_{scl}\mathbf{N}_{abcs}(\boldsymbol{K_s})^{-1} \\ c_{scl}\boldsymbol{K_s}\mathbf{N}^\top_{abcs} & \mathbf{0} \end{bmatrix} \begin{bmatrix} \boldsymbol{\Phi} \\ \boldsymbol{i}_{qd0s}/c_{scl} \end{bmatrix} = \begin{bmatrix} \mathbf{N}_{fld} & \mathbf{0} \\ \mathbf{0} & c_{scl}\boldsymbol{I}_3/P \end{bmatrix} \begin{bmatrix} i_{fld} \\ \boldsymbol{\lambda}_{qd0s} \end{bmatrix}. \tag{3}$$

The idea is to incorporate the machine dynamics into the otherwise static relation of current and flux in (1). $\boldsymbol{i}_{qd0s}$ and $\boldsymbol{\lambda}_{qd0s}$ are the currents and flux linkages of the stator windings in the rotor reference frame. $\boldsymbol{z}_{qd0} = \boldsymbol{K_s}\boldsymbol{z}_{abc}$, where $\boldsymbol{z}$ represents flux linkages, currents, or voltages, and $\boldsymbol{K_s}$ is the reference frame transformation matrix [1]. $\mathbf{N}_{fld}$ is the turns matrix for the field winding. i_{fld} is the field current. c_{scl} is a scaling factor to condition (3). Equation (3) can be solved to obtain currents, $\boldsymbol{i}_{qd0s}$, for given flux linkages, $\boldsymbol{\lambda}_{qd0s}$.

State-space representation of a synchronous machine in the rotor reference-frame is [1]

$$\frac{d\lambda_{qs}}{dt} = v_{qs} - r_s i_{qs} - \omega_r \lambda_{ds}, \tag{4a}$$

$$\frac{d\lambda_{ds}}{dt} = v_{ds} - r_s i_{ds} + \omega_r \lambda_{qs}, \tag{4b}$$

$$\frac{d\lambda_{0\,s}}{dt} = v_{0\,s} - r_s i_{0\,s}. \tag{4c}$$

v_{qs}, v_{ds}, and $v_{0\,s}$ are the q-axis, d-axis, and 0-axis voltage terms. r_s is the stator resistance, and ω_r is the rotor speed. Dynamic MEC model solves (3) and (4) in tandem. The electromagnetic torque is calculated using [5]

$$T_e^{\mathrm{MEC}} = \left(\frac{P}{2}\right)^2 \sum_{j=1}^{na} \left(\frac{\phi_{aj}}{P_{aj}}\right)^2 \frac{\partial P_{aj}}{\partial \theta_r}, \tag{5}$$

where ϕ_{aj} and P_{aj} represent flux and permeance for the jth loop in the airgap region. na is the number of airgap loops (changing with the rotor position), and θ_r is the rotor position.

B. $qd0$ Model

State-space representation of a lumped-parameter model is the same as (4). However, the relation between flux linkages and currents is formulated as [1]

$$\lambda_{qs} = (L_{ls} + L_{mq}) i_{qs}, \tag{6a}$$

$$\lambda_{ds} = (L_{ls} + L_{md}) i_{ds} + \frac{2}{3}\frac{N_{fld}}{N_s} L_{md} i_{fld}, \tag{6b}$$

$$\lambda_{0\,s} = L_{ls} i_{0\,s}. \tag{6c}$$

L_{ls} is the leakage inductance of stator, L_{mq} and L_{md} are the q- and d-axis magnetizing inductances, respectively. N_{fld} and N_s are the lumped equivalency of spatially-distributed field winding and stator winding, respectively. The electromagnetic torque becomes

$$T_e = \frac{3P}{4}(\lambda_{ds} i_{qs} - \lambda_{qs} i_{ds}). \tag{7}$$

$qd0$ parameter extraction from the MEC model is analogous to replacing the flux linkage and current relation in (3) with (6).

IV. Setting up the Model Extraction Procedure

In order to extract the $qd0$ model from the MEC model, one can compare trajectories generated from (3), (4), and (5) with those predicted by (6), (4), and (7) and minimize their mismatch. This requires one to discretize the $qd0$ model.

A. Discretizing Machine Dynamics

While a host of methods are available, (e.g., Tustin's [27]), in this work, the forward Euler method is adopted for its simplicity. The discretized state trajectory for a general dynamic system $\frac{d\mathbf{x}}{dt} = f(\mathbf{x})$ using the forward Euler method is

$$\mathbf{x}[\tau + 1] = \mathbf{x}[\tau] + \Delta T \times f(\mathbf{x}). \tag{8}$$

$\mathbf{x}$ is the state, ΔT is the sampling time, and τ is the time instance. The $qd0$ model in (4), (6), and (7) is discretized as

$$\boldsymbol{\lambda}[\tau + 1] = \boldsymbol{A}\boldsymbol{\lambda}[\tau] + \boldsymbol{R}\boldsymbol{i}[\tau] + \boldsymbol{v}[\tau], \tag{9a}$$

$$\boldsymbol{\lambda}[\tau] = \boldsymbol{L}\boldsymbol{i}[\tau] + \boldsymbol{\ell}\, i_{fld}, \tag{9b}$$

$$Q \times T_e[\tau] = \frac{3}{4}\boldsymbol{\lambda}^\top[\tau]\boldsymbol{M}\boldsymbol{i}[\tau]. \tag{9c}$$

$\boldsymbol{\lambda}[\tau] \in \mathbb{R}^3$ and $\boldsymbol{i}[\tau] \in \mathbb{R}^3$ are the flux linkages and currents, respectively, in the rotor reference frame at time instance τ. The $qd0$ subscript is dropped for brevity. $\boldsymbol{v}[\tau]$ in (9a) is the $qd0$ voltage terms times the sampling time, $\boldsymbol{v}[\tau] = \boldsymbol{v}_{qd0}[\tau] \times \Delta T$. Matrices $\boldsymbol{A}$, $\boldsymbol{R}$, $\boldsymbol{L}$, $\boldsymbol{\ell}$, $\boldsymbol{M}$, and Q in (9) are defined as

$$\boldsymbol{A} \triangleq \begin{bmatrix} 1 & -a & 0 \\ a & 1 & 0 \\ 0 & 0 & 1 \end{bmatrix}, \quad \boldsymbol{R} \triangleq \begin{bmatrix} -r & 0 & 0 \\ 0 & -r & 0 \\ 0 & 0 & -r \end{bmatrix}, \tag{10a}$$

$$Q \triangleq \frac{1}{P}, \qquad \boldsymbol{L} \triangleq \begin{bmatrix} l_1 & 0 & 0 \\ 0 & l_2 & 0 \\ 0 & 0 & l_3 \end{bmatrix}, \tag{10b}$$

$$\boldsymbol{\ell} \triangleq \begin{bmatrix} 0 \\ l_4 \\ 0 \end{bmatrix}, \quad \boldsymbol{M} \triangleq \begin{bmatrix} 0 & -1 & 0 \\ 1 & 0 & 0 \\ 0 & 0 & 0 \end{bmatrix}, \tag{10c}$$

where $a \triangleq \omega_r \Delta T$, $r \triangleq r_s \Delta T$, $l_1 \triangleq L_{ls} + L_{mq}$, $l_2 \triangleq L_{ls} + L_{md}$, $l_3 \triangleq L_{ls}$, and $l_4 \triangleq \frac{2}{3}\frac{N_{fld}}{N_s} L_{md}$. The model extraction problem presented in following sections aims to determine the values $(a, r, l_1, l_2, l_3, l_4, Q)$ based on which machine parameters, ω_r, r_s, L_{ls}, L_{mq}, L_{md}, $\frac{N_{fld}}{N_s}$, and P can be uniquely determined.

B. Problem Formulation

Suppose that we are given the vectors $\boldsymbol{\lambda}^{\text{MEC}}[\tau]$, $\boldsymbol{i}^{\text{MEC}}[\tau]$, and $T_e^{\text{MEC}}[\tau]$ throughout a discrete time horizon $\tau \in \{1, 2, \ldots, \mathfrak{t}\}$, representing flux linkages, currents, and torque data from the MEC model, respectively. Then, the parameter extraction for a $qd0$ model from the MEC data can be formulated as the following optimization problem:

$$\textbf{minimize} \sum_{\tau=1}^{\mathfrak{t}} \left\| \boldsymbol{\lambda}[\tau] - \boldsymbol{\lambda}^{\text{MEC}}[\tau] \right\|_{\boldsymbol{\lambda}_\alpha}^2 + \sum_{\tau=1}^{\mathfrak{t}} \left\| \boldsymbol{i}[\tau] - \boldsymbol{i}^{\text{MEC}}[\tau] \right\|_{\boldsymbol{\lambda}_\beta}^2 + \sum_{\tau=1}^{\mathfrak{t}} \gamma \left(T_e[\tau] - T_e^{\text{MEC}}[\tau] \right)^2 \tag{11a}$$

subject to

$$\boldsymbol{\lambda}[\tau + 1] = \boldsymbol{\lambda}[\tau] + a \times [-\lambda_2[\tau], \lambda_1[\tau], 0]^\top - r \times \boldsymbol{i}[\tau] + \boldsymbol{v}[\tau], \quad \tau = 1, 2, \ldots, \mathfrak{t} - 1 \tag{11b}$$

$$\boldsymbol{\lambda}[\tau] = \text{diag}\{[l_1, l_2, l_3]\}\boldsymbol{i}[\tau] + [0,\ l_4,\ 0]^\top \times i_{fld}, \quad \tau = 1, 2, \ldots, \mathfrak{t} \tag{11c}$$

$$Q \times T_e[\tau] = \frac{3}{4}\boldsymbol{\lambda}^\top[\tau]\,[-i_2[\tau], i_1[\tau], 0]^\top, \tau = 1, 2, \ldots, \mathfrak{t}$$

variables

$$\left\{ \boldsymbol{\lambda}[\tau] \in \mathbb{R}^3, \boldsymbol{i}[\tau] \in \mathbb{R}^3, T_e[\tau] \in \mathbb{R} \right\}_{\tau=1}^{\mathfrak{t}},$$
$$a, l_1, l_2, l_3, l_4, r, Q \in \mathbb{R}. \tag{11d}$$

The 3×3 matrices $\boldsymbol{\Lambda}_\alpha$ and $\boldsymbol{\Lambda}_\beta$ are defined as

$$\boldsymbol{\Lambda}_\alpha \triangleq \begin{bmatrix} \alpha_1 & 0 & 0 \\ 0 & \alpha_2 & 0 \\ 0 & 0 & \alpha_3 \end{bmatrix}, \quad \boldsymbol{\Lambda}_\beta \triangleq \begin{bmatrix} \beta_1 & 0 & 0 \\ 0 & \beta_2 & 0 \\ 0 & 0 & \beta_3 \end{bmatrix}. \tag{12}$$

$(\alpha_1, \alpha_2, \alpha_3)$, $(\beta_1, \beta_2, \beta_3)$ and γ are user-defined non-negative weights given to flux, current and torque data, respectively.

The objective function in (11a) represents the total mismatch between the MEC and $qd0$ trajectories. The equality constraint in (11b) represents the state equation for the $qd0$ model. Constraints in (11c) and (11d) form the flux linkage-current relationship and torque expressions, respectively. The auxiliary variable

$Q = 1/P$ is defined to reduce the order of torque equation from three (cubic) to two (quadratic), which will help in the following convex formulation. To summarize, the optimization problem in (11) minimizes the sum of scaled residuals for trajectories of flux linkages, currents, and torque to uniquely obtain $\boldsymbol{\lambda}$, $\boldsymbol{i}$, T_e, $\boldsymbol{A}$, $\boldsymbol{R}$, $\boldsymbol{L}$, $\boldsymbol{\ell}$, and Q subject to the constraints in (11a)–(11d).

V. Convex Relaxation and Numerical Search

Without proper initialization, local search algorithms may fail to converge to a globally optimal solution or even a feasible point. To address this issue, we use cone programming relaxation followed by IPM to reliably solve the problem (11a)–(11d). The proposed convex relaxation is explained next.

A. Cone Programming Relaxation

The original optimization problem in (11) is non-convex due to the presence of bilinear terms:

- $a\ \lambda_2[\tau]$, $a\ \lambda_1[\tau]$ and $r\ \boldsymbol{i}[\tau]$ in (11b);
- $l_1\ i_1[\tau]$, $l_2\ i_2[\tau]$ and $l_3\ i_3[\tau]$ in (11c); as well as
- $\lambda_1[\tau]\ i_2[\tau]$, $\lambda_2[\tau]\ i_1[\tau]$ and $Q\ T_e[\tau]$ in (11d).

The aforementioned nonlinearity can be tackled by introducing new variable (i.e., lifting the problem). To this end, define

$$\boldsymbol{f}[\tau] \triangleq [a\lambda_2[\tau],\ -a\lambda_1[\tau],\ 0]^\top, \tag{13a}$$

$$\boldsymbol{h}[\tau] \triangleq r \times \boldsymbol{i}[\tau], \tag{13b}$$

$$\boldsymbol{z}[\tau] \triangleq \mathrm{diag}\{[l_1,\ l_2,\ l_3]\}\ \boldsymbol{i}[\tau], \tag{13c}$$

$$\boldsymbol{w}[\tau] \triangleq [\lambda_1[\tau]i_2[\tau], \lambda_2[\tau]i_1[\tau],\ 0]^\top, \tag{13d}$$

$$\theta[\tau] \triangleq Q \times T_e[\tau]. \tag{13e}$$

The aforementioned auxiliary terms participate in (11b)–(11d) and can be used to simplify them, as we will demonstrate later. However, in order to streamline the relaxation process, it is necessary to reformulate the definitions in (13) as follows:

$$\sqrt{(\bar{a} - a^2)\left(\bar{\lambda}_2[\tau] - \lambda_2[\tau]^2\right)} = |f_1[\tau] - a\lambda_2[\tau]|,$$

$$\sqrt{(\bar{a} - a^2)\left(\bar{\lambda}_1[\tau] - \lambda_1[\tau]^2\right)} = |f_2[\tau] + a\lambda_1[\tau]|,$$

$$f_3[\tau] = 0 \qquad \tau = 1, 2, \ldots, \mathrm{t} \tag{14a}$$

$$\sqrt{\left(\bar{\lambda}_1[\tau] - \lambda_1[\tau]^2\right)\left(\bar{i}_2[\tau] - i_2[\tau]^2\right)} = |w_1[\tau] - \lambda_1[\tau]i_2[\tau]|,$$

$$\sqrt{\left(\bar{\lambda}_2[\tau] - \lambda_2[\tau]^2\right)\left(\bar{i}_1[\tau] - i_1[\tau]^2\right)} = |w_2[\tau] - \lambda_2[\tau]i_1[\tau]|,$$

$$w_3[\tau] = 0 \qquad \tau = 1, 2, \ldots, \mathrm{t} \tag{14b}$$

$$\sqrt{\mathrm{diag}\{[\bar{l}_1 - l_1^2,\ \bar{l}_2 - l_2^2,\ \bar{l}_3 - l_3^2]\}(\bar{\boldsymbol{i}}[\tau] - \mathrm{diag}\{\boldsymbol{i}[\tau]\}\boldsymbol{i}[\tau])}$$
$$= |\boldsymbol{z}[\tau] - \mathrm{diag}\{[l_1,\ l_2,\ l_3]\}\ \boldsymbol{i}[\tau]| \quad \tau = 1, 2, \ldots, \mathrm{t} \tag{14c}$$

$$\sqrt{(\bar{r} - r^2)(\bar{\boldsymbol{i}}[\tau] - \mathrm{diag}\{\boldsymbol{i}[\tau]\}\boldsymbol{i}[\tau])}$$
$$= |\boldsymbol{h}[\tau] - r \times \boldsymbol{i}[\tau]| \qquad \tau = 1, 2, \ldots, \mathrm{t} \tag{14d}$$

$$\sqrt{(\bar{Q} - Q^2)(\bar{T}_e[\tau] - T_e[\tau]^2)}$$
$$= |\theta[\tau] - Q \times \bar{T}_e[\tau]| \qquad \tau = 1, 2, \ldots, \mathrm{t} \tag{14e}$$

where

$$\bar{l}_1 \triangleq l_1^2, \quad \bar{l}_2 \triangleq l_3^2, \quad \bar{l}_3 \triangleq l_3^2, \tag{15a}$$

$$\bar{a} \triangleq a^2, \quad \bar{r} \triangleq r^2, \quad \bar{Q} \triangleq Q^2, \tag{15b}$$

$$\bar{\boldsymbol{\lambda}}[\tau] \triangleq \mathrm{diag}\{\boldsymbol{\lambda}[\tau]\}\boldsymbol{\lambda}[\tau], \qquad \tau = 1, 2, \ldots, \mathrm{t} \tag{15c}$$

$$\bar{\boldsymbol{i}}[\tau] \triangleq \mathrm{diag}\{\boldsymbol{i}[\tau]\}\boldsymbol{i}[\tau], \qquad \tau = 1, 2, \ldots, \mathrm{t} \tag{15d}$$

$$\bar{T}_e[\tau] \triangleq T_e[\tau]^2. \qquad \tau = 1, 2, \ldots, \mathrm{t} \tag{15e}$$

It can be observed that the equations in (14) are equivalent to (13). In what follows, we will transform all of equalities in (14) and (15), in order to arrive to a convex relaxation:

$$\textbf{minimize} \sum_{\tau=1}^{\mathrm{t}} \boldsymbol{\alpha}^\top \left(\bar{\boldsymbol{\lambda}}[\tau] + \mathrm{diag}\{\boldsymbol{\lambda}^{\mathrm{MEC}}[\tau]\}(\boldsymbol{\lambda}^{\mathrm{MEC}}[\tau] - 2\boldsymbol{\lambda}[\tau])\right)$$
$$+ \sum_{\tau=1}^{\mathrm{t}} \boldsymbol{\beta}^\top \left(\bar{\boldsymbol{i}}[\tau] + \mathrm{diag}\{\boldsymbol{i}^{\mathrm{MEC}}[\tau]\}(\boldsymbol{i}^{\mathrm{MEC}}[\tau] - 2\boldsymbol{i}[\tau])\right)$$
$$+ \sum_{\tau=1}^{\mathrm{t}} \gamma \left(\bar{T}_e[\tau] - 2\ T_e^{\mathrm{MEC}}[\tau]T_e[\tau] + T_e^{\mathrm{MEC}}[\tau]^2\right) \tag{16a}$$

subject to

$$\boldsymbol{\lambda}[\tau + 1] = \boldsymbol{\lambda}[\tau] - \boldsymbol{f}[\tau] - \boldsymbol{h}[\tau] + \boldsymbol{v}[\tau], \qquad \tau = 1, 2, \ldots, \mathrm{t} - 1 \tag{16b}$$

$$\boldsymbol{\lambda}[\tau] = \boldsymbol{z}[\tau] + [0,\ l_4,\ 0]^\top \times i_{fld}, \qquad \tau = 1, 2, \ldots, \mathrm{t} \tag{16c}$$

$$\theta[\tau] = \frac{3}{4}(w_2[\tau] - w_1[\tau]), \qquad \tau = 1, 2, \ldots, \mathrm{t} \tag{16d}$$

$$\bar{l}_1 \geq l_1^2, \quad \bar{l}_2 \geq l_3^2, \quad \bar{l}_3 \geq l_3^2, \tag{16e}$$

$$\bar{a} \geq a^2, \quad \bar{r} \geq r^2, \quad \bar{Q} \geq Q^2, \tag{16f}$$

$$\bar{\boldsymbol{\lambda}}[\tau] \geq \mathrm{diag}\{\boldsymbol{\lambda}[\tau]\}\boldsymbol{\lambda}[\tau], \qquad \tau = 1, 2, \ldots, \mathrm{t} \tag{16g}$$

$$\bar{\boldsymbol{i}}[\tau] \geq \mathrm{diag}\{\boldsymbol{i}[\tau]\}\boldsymbol{i}[\tau], \qquad \tau = 1, 2, \ldots, \mathrm{t} \tag{16h}$$

$$\bar{T}_e[\tau] \geq T_e[\tau]^2 \qquad \tau = 1, 2, \ldots, \mathrm{t} \tag{16i}$$

$$\sqrt{(\bar{a} - a^2)\left(\bar{\lambda}_2[\tau] - \lambda_2[\tau]^2\right)} \geq |f_1[\tau] - a\lambda_2[\tau]|,$$

$$\sqrt{(\bar{a} - a^2)\left(\bar{\lambda}_1[\tau] - \lambda_1[\tau]^2\right)} \geq |f_2[\tau] + a\lambda_1[\tau]|,$$

$$f_3[\tau] = 0 \qquad \tau = 1, 2, \ldots, \mathrm{t} \tag{16j}$$

$$\sqrt{\left(\bar{\lambda}_1[\tau] - \lambda_1[\tau]^2\right)\left(\bar{i}_2[\tau] - i_2[\tau]^2\right)} \geq |w_1[\tau] - \lambda_1[\tau]i_2[\tau]|,$$

$$\sqrt{\left(\bar{\lambda}_2[\tau] - \lambda_2[\tau]^2\right)\left(\bar{i}_1[\tau] - i_1[\tau]^2\right)} \geq |w_2[\tau] - \lambda_2[\tau]i_1[\tau]|,$$

$$w_3[\tau] = 0 \qquad \tau = 1, 2, \ldots, \mathrm{t} \tag{16k}$$

$$\sqrt{\mathrm{diag}\{[\bar{l}_1 - l_1^2,\ \bar{l}_2 - l_2^2,\ \bar{l}_3 - l_3^2]\}(\bar{\boldsymbol{i}}[\tau] - \mathrm{diag}\{\boldsymbol{i}[\tau]\}\boldsymbol{i}[\tau])}$$
$$\geq |\boldsymbol{z}[\tau] - \mathrm{diag}\{[l_1,\ l_2,\ l_3]\}\ \boldsymbol{i}[\tau]| \quad \tau = 1, 2, \ldots, \mathrm{t} \tag{16l}$$

$$\sqrt{(\bar{r} - r^2)(\bar{\boldsymbol{i}}[\tau] - \mathrm{diag}\{\boldsymbol{i}[\tau]\}\boldsymbol{i}[\tau])}$$
$$\geq |\boldsymbol{h}[\tau] - r \times \boldsymbol{i}[\tau]| \qquad \tau = 1, 2, \ldots, \mathrm{t} \tag{16m}$$

$$\sqrt{(\bar{Q}-Q^2)(\bar{T}_e[\tau]-T_e[\tau]^2)} \geq |\theta[\tau]-Q\times\bar{T}_e[\tau]| \qquad \tau=1,2,\ldots,\mathfrak{t} \quad (16n)$$

variables

$$\left\{\boldsymbol{\lambda}[\tau],\boldsymbol{i}[\tau],\bar{\boldsymbol{\lambda}}[\tau],\bar{\boldsymbol{i}}[\tau],\boldsymbol{f}[\tau],\boldsymbol{h}[\tau],\boldsymbol{z}[\tau],\boldsymbol{w}[\tau]\in\mathbb{R}^3\right\}_{\tau=1}^{\mathfrak{t}},$$

$$\left\{T_e[\tau],\bar{T}_e[\tau]\in\mathbb{R}\right\}_{\tau=1}^{\mathfrak{t}},$$

$$a,l_1,l_2,l_3,l_4,r,Q,\bar{a},\bar{l}_1,\bar{l}_2,\bar{l}_3,\bar{r},\bar{Q}\in\mathbb{R}.$$

The non-negative weights in the objective function in (16a) are $\boldsymbol{\alpha}=\mathrm{diag}(\boldsymbol{\Lambda}_\alpha)$ and $\boldsymbol{\beta}=\mathrm{diag}(\boldsymbol{\Lambda}_\beta)$. Equality constraints in (16b)–(16d) are the same as those in (11b)–(11d) which describe the WRSM model equations. The inequalities in (16e)–(16k) implicitly impose (13)–(15) to preserve equivalency to the original problem in (11) and the convexified problem in (16). It is straightforward to observe that (16e)–(16k) are convex if formulated as linear matrix inequalities:

$$\begin{bmatrix}\bar{a} & f_k[\tau]\\ f_k[\tau] & \bar{\lambda}_{3-k}[\tau]\end{bmatrix}\succeq\begin{bmatrix}(-1)^{3-k}a\\ \lambda_{3-k}[\tau]\end{bmatrix}\begin{bmatrix}(-1)^{3-k}a\\ \lambda_{3-k}[\tau]\end{bmatrix}^\top \qquad k=1,2 \quad (17a)$$

$$\begin{bmatrix}\bar{\lambda}_k[\tau] & w_k[\tau]\\ w_k[\tau] & \bar{i}_{3-k}[\tau]\end{bmatrix}\succeq\begin{bmatrix}\lambda_k[\tau]\\ i_{3-k}[\tau]\end{bmatrix}\begin{bmatrix}\lambda_k[\tau]\\ i_{3-k}[\tau]\end{bmatrix}^\top \qquad k=1,2 \quad (17b)$$

$$\begin{bmatrix}\bar{l}_k & z_k[\tau]\\ z_k[\tau] & \bar{i}_k[\tau]\end{bmatrix}\succeq\begin{bmatrix}l_k\\ i_k[\tau]\end{bmatrix}\begin{bmatrix}l_k\\ i_k[\tau]\end{bmatrix}^\top \qquad k=1,2,3 \quad (17c)$$

$$\begin{bmatrix}\bar{r} & h_k[\tau]\\ h_k[\tau] & \bar{i}_k[\tau]\end{bmatrix}\succeq\begin{bmatrix}r\\ i_k[\tau]\end{bmatrix}\begin{bmatrix}r\\ i_k[\tau]\end{bmatrix}^\top \qquad k=1,2,3 \quad (17d)$$

$$\begin{bmatrix}\bar{Q} & \theta[\tau]\\ \theta[\tau] & \bar{T}_{e,k}[\tau]\end{bmatrix}\succeq\begin{bmatrix}Q\\ T_{e,k}[\tau]\end{bmatrix}\begin{bmatrix}Q\\ T_{e,k}[\tau]\end{bmatrix}^\top \qquad k=1,2,3 \quad (17e)$$

The optimization problem in (16) is a relaxation and its solution may not be feasible for the original problem in (11). Nonetheless, the solution of convex relaxation can be used as an initial point for any general-purpose IPM solver.

As an alternative to IPM, [28] proposes a penalization method to find feasible and near-optimal solutions to problems of the form (11). This approach is regarded as penalized convex relaxation. Let $\hat{\boldsymbol{x}}=(\{\hat{\boldsymbol{\lambda}}[\tau],\hat{\boldsymbol{i}}[\tau],\hat{T}_e[\tau]\}_{\tau=1}^{\mathfrak{t}},\hat{a},\hat{l}_1,\hat{l}_2,\hat{l}_3,\hat{r},\hat{Q})$ be an optimal solution for the convex problem (16). If $\hat{\boldsymbol{x}}$ is not feasible for the original nonconvex problem, one can incorporate a penalty term of the form

$$\begin{aligned}&\kappa\left(\{\hat{\boldsymbol{\lambda}}[\tau],\hat{\boldsymbol{i}}[\tau],\hat{T}_e[\tau]\}_{\tau=1}^{\mathfrak{t}},\hat{a},\hat{l}_1,\hat{l}_2,\hat{l}_3,\hat{r},\hat{Q}\right)\\ &=\eta_a(\bar{a}-2\hat{a}a+\hat{a}^2)+\eta_r(\bar{r}-2\hat{r}r+\hat{r}^2)\\ &\quad+\eta_Q(\bar{Q}-2\hat{Q}Q+\hat{Q}^2)+\eta_{l_1}(\bar{l}_1-2\hat{l}_1l_1+\hat{l}_1^2)\\ &\quad+\eta_{l_2}(\bar{l}_2-2\hat{l}_2l_2+\hat{l}_2^2)+\eta_{l_3}(\bar{l}_3-2\hat{l}_3l_3+\hat{l}_3^2)\\ &\quad+\eta_\lambda\sum_{\tau=1}^{\mathfrak{t}}(\mathbf{1}_3^\top\bar{\boldsymbol{\lambda}}[\tau]-2\hat{\boldsymbol{\lambda}}^\top[\tau]\boldsymbol{\lambda}[\tau]+\hat{\boldsymbol{\lambda}}^\top[\tau]\hat{\boldsymbol{\lambda}}[\tau])\\ &\quad+\eta_i\sum_{\tau=1}^{\mathfrak{t}}(\mathbf{1}_3^\top\bar{\boldsymbol{i}}[\tau]-2\hat{\boldsymbol{i}}^\top[\tau]\boldsymbol{i}[\tau]+\hat{\boldsymbol{i}}^\top[\tau]\hat{\boldsymbol{i}}[\tau])\\ &\quad+\eta_{T_e}\sum_{\tau=1}^{\mathfrak{t}}(\bar{T}_e[\tau]-2\hat{T}_e[\tau]T_e[\tau]+\hat{T}_e^2), \end{aligned} \quad (18)$$

in the objective function of relaxation, and solve additional rounds to obtain fully feasible points with satisfactory objective values. In (18), the parameters $\eta_a,\eta_r,\eta_Q,\eta_{l_1},\eta_{l_2},\eta_{l_3},\eta_\lambda,\eta_i,\eta_{T_e}\geq 0$ are user-defined.

VI. Model Generation and Verification

A. System Setup

The MEC model of a 2 kW WRSM is adopted from [3]. The machine is constructed using M19 steel laminations, and copper conductors are used for stator and field windings. The optimization experiments are run on a workstation equipped with Intel(R) Core i7-6700 CPU (4 cores) at 3.40 GHz and 32 GB of RAM with Windows 10. The conic optimization problem in (16) is solved using the SDPT3 4.0 [29] and MOSEK [30] solver running on CVX [31] in the MATLAB 2017b environment. Local search is implemented using MATPOWER Interior Point Solver (MIPS) [32].

B. Training Data Generated by the Dynamic MEC Model

We have considered an unbalanced operation of the WRSM to generate training data with non-zero zero-sequence flux linkage and current components. Zero initial conditions are assumed for the states. Fig. 2 shows the flux linkages, currents, and electromagnetic torque waveforms generated using the MEC model. The highlighted portions of plots in Fig. 2, that include 100 data points, are used in parameter extraction. More data points will improve the solution, albeit at the expense of computational time.

C. Model Extraction Procedure

The optimization problem in Section V-A is first solved using cone programming relaxation. The result is used as an initial condition for IPM. The tuning gains for the relaxed problem are $\Lambda_{\boldsymbol{\alpha}}=\Lambda_{\boldsymbol{\beta}}=\mathbf{diag}\{1,1,0.001\}$ and $\gamma=1$. A flat initial condition is assumed with all unknown variables set to 1. The length of the time horizon is $\mathfrak{t}=100$. Conic relaxation solves (16) over a convexified version of the feasible set of (11). Table I shows the relaxation results. The obtained set is not necessarily a feasible point (e.g., see L_{ls}), but can be a good initial point for IPM. In comparison, in all of our experiments, five rounds of penalized relaxation (see (18)) resulted in feasible points and parameters similar to those of IPM.

The tuning gains for IPM are $\Lambda_{\boldsymbol{\alpha}}=\mathbf{diag}\{10^4,10^4,10^4\}$, $\Lambda_{\boldsymbol{\beta}}=\mathbf{diag}\{0.001,0.001,0.001\}$, and $\gamma=0.1$. Table II tabulates the parameters extracted by IPM after solving (11). These

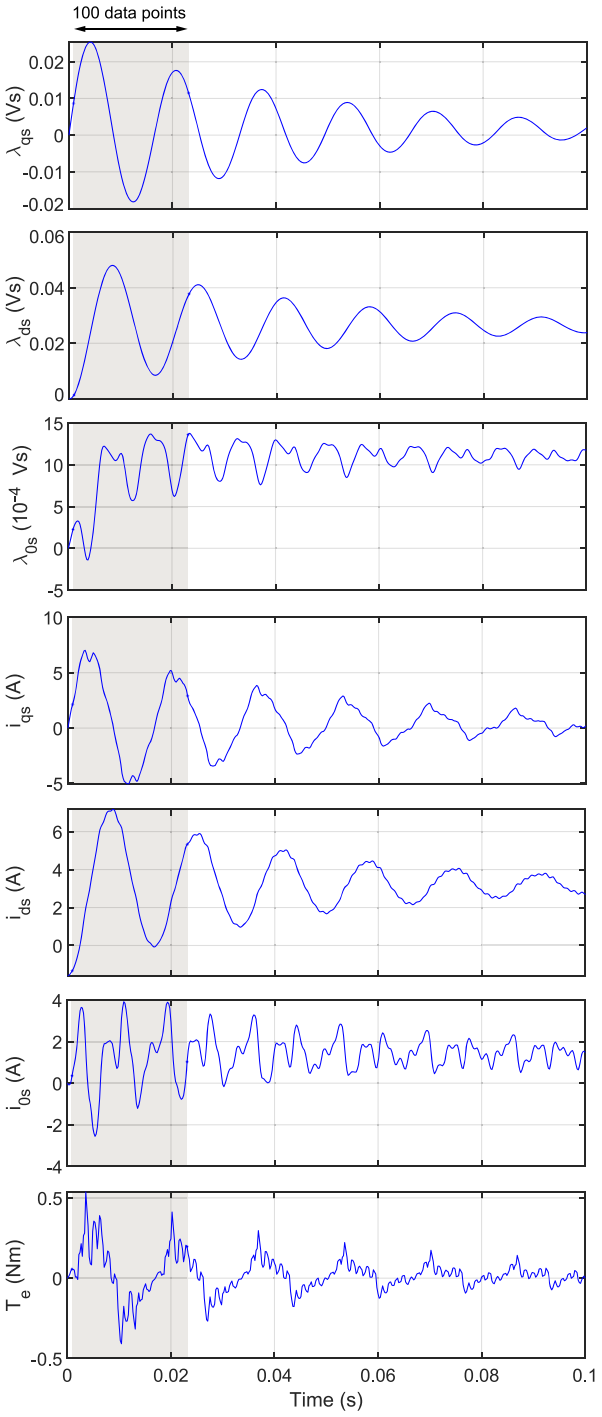

Fig. 2. Time-domain transients for flux linkages, currents, and electromagnetic torque. Operating condition is $i_{fld} = 0.25$ A, $\omega_r = 3600$ RPM, $v_{qs} = 10$ V, $v_{ds} = 0$ V, and $v_{0s} = 0.25$ V. The sampling length is $\Delta T = 2.22 \times 10^{-4}$ s. Only the highlighted sections of the data are used for model extraction.

parameters are compared against those reported in [3] (corresponding to MEC-BH1 model). Reference value of the stator resistance, $r_s = 0.1729\ \Omega$, is directly obtained in the MEC model [3] using equivalent length and area of the windings. The reference value for the effective turns ratio between the field and stator windings, $\frac{N_{fld}}{N_s}$, is taken from that reported in [33]. As seen in Table II, the percentage mismatch for the estimated

TABLE I
INITIAL PARAMETERS OBTAINED USING A SINGLE RUN OF CONVEX RELAXATION: MEC-BH1 (t = 100)

Parameter	MEC [3], [33]	Estimated Parameters	%Mismatch (w.r.t. MEC model)
ω_r*(rad/sec)	376.99	376.98	0.0005
$r_s(\Omega)$	0.1729**	0.1729	0
L_{ls} (mH)	0.83	0.27	67.47
L_{mq} (mH)	3.06	3.38	10.45
L_{md} (mH)	4.71	5.19	10.19
$\frac{N_{fld}}{N_s}$	10.94	10.23	6.50
P	4	4.44***	-

*Electrical angular speed of the rotor. **Directly obtained from the MEC model. ***The number of poles, P, takes even integers.

TABLE II
MACHINE PARAMETERS EXTRACTED USING HYBRID CONE PROGRAMMING RELAXATION AND IPM: MEC-BH1 (t = 100)

Parameter	MEC [3], [33]	Hardware [3]	Estimated Parameters	%Mismatch (wrt MEC/Hardware)
ω_r*(rad/sec)	376.99	376.99	377.10	0.02 / 0.02
$r_s(\Omega)$	0.1729**	0.21	0.1738	0.52 / 17.23
L_{ls} (mH)	0.83	0.90	0.75	9.06 / 16.13
L_{mq} (mH)	3.06	3.07	2.94	3.74 / 4.05
L_{md} (mH)	4.71	4.46	4.74	0.66 / 6.30
$\frac{N_{fld}}{N_s}$	10.94	Not available	11.16	2.00 / -
P	4	4	3.90***	- / -

*Electrical angular speed of the rotor. **Directly obtained from the MEC model. ***The number of poles, P, takes even integers.

TABLE III
MACHINE PARAMETERS EXTRACTED USING HYBRID CONE PROGRAMMING RELAXATION AND IPM: MEC-BH2 (t = 100)

Parameter	MEC [3], [33]	Hardware [3]	Estimated Parameters	%Mismatch (wrt MEC/Hardware)
ω_r*(rad/sec)	376.99	376.99	377.12	0.03 / 0.03
$r_s(\Omega)$	0.1729**	0.21	0.1737	0.46 / 17.28
L_{ls} (mH)	0.82	0.90	0.74	9.75 / 17.77
L_{mq} (mH)	2.94	3.07	2.84	3.40 / 7.49
L_{md} (mH)	4.33	4.46	4.34	0.23 / 2.69
$\frac{N_{fld}}{N_s}$	10.94	Not available	11.35	3.75 / -
P	4	4	3.89***	- / -

*Electrical angular speed of the rotor. **Directly obtained from the MEC model. ***The number of poles, P, takes even integers.

parameters w.r.t. MEC reference values is highest for L_{ls} at 9.06%, whereas the rest of the parameters are estimated within 3.8% accuracy. Estimation error with respect to the hardware values is obviously higher given the inherent mismatch between the original MEC model and the hardware prototype in [3]. It should be noted that parameters reported for MEC model should be considered for comparative purpose. [3] also proposed a second MEC model of WRSM, named MEC-BH2, to address the discrepancy between the anhysteretic *BH* curve used in the MEC model and *BH* curve obtained from the material used in the machine design. For completion, results for parameter extraction on MEC-BH2 model are also provided in Table III.

In the problem formulation in (11) and (16), transients of flux linkages, currents, and electromagnetic torque are also

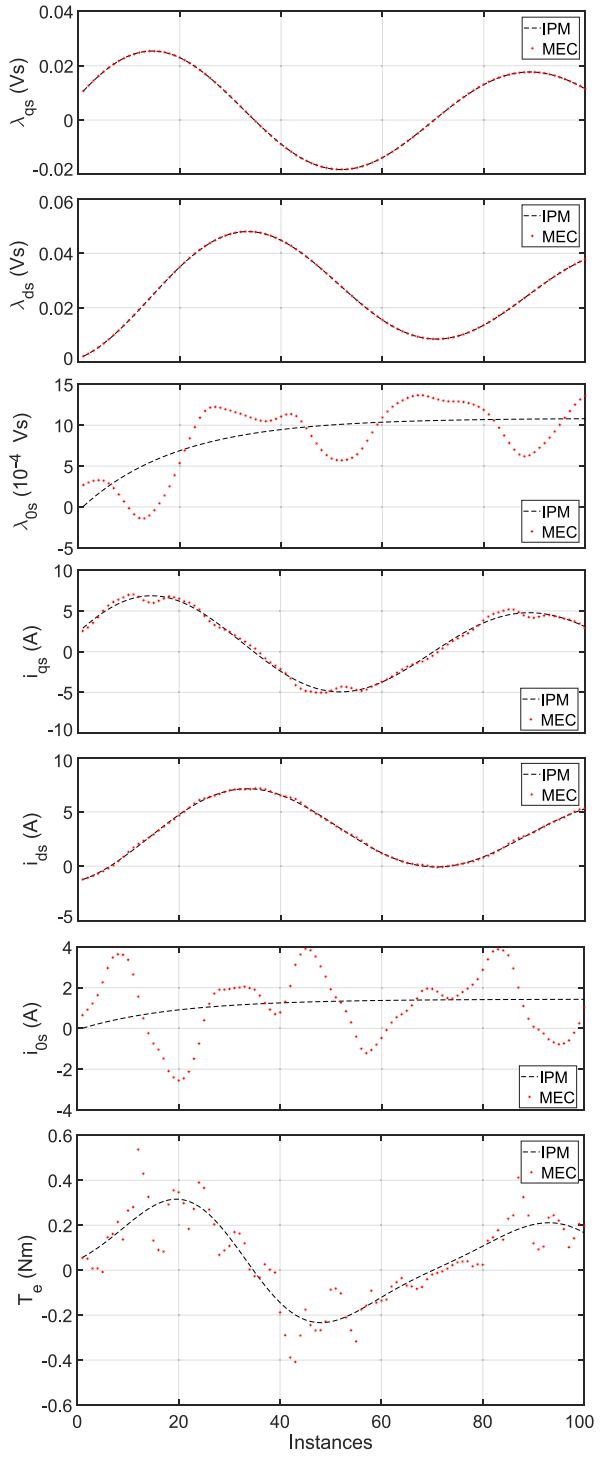

Fig. 3. Trajectories obtained from IPM compared with the MEC data for MEC-BH1 using t = 100. Apart from the machine parameters listed in Table II, transients of flux linkages (λ_{qs}, λ_{ds}, λ_{0s}), currents (i_{qs}, i_{ds}, i_{0s}), and electromagnetic torque (T_e) are also obtained from the solution to the optimization problem.

considered as optimization variables. The IPM solution recovers these variables along with the machine parameters. Fig. 3 compares the time-domain transients of input MEC data and the trajectories obtained by the optimization process for MEC-BH1. The red curves in Fig. 3 show the data from the MEC model that

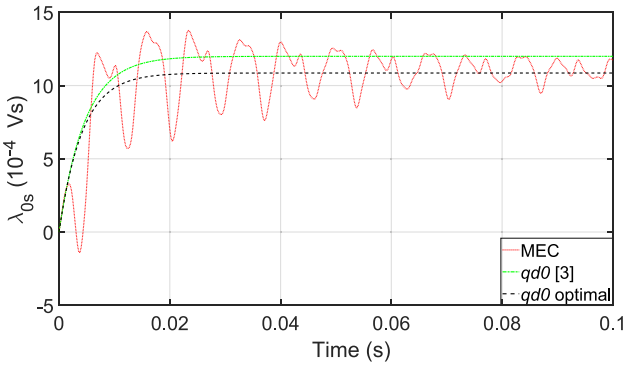

Fig. 4. Zero-sequence flux linkage transients from MEC model (red), and two *qd0* models with parameters obtained from [3] and using the proposed method.

TABLE IV
COMPUTATIONS AND TIME DURATIONS FOR HYBRID CONE PROGRAMMING RELAXATION AND IPM

Test Case	Iterations		Running Time		
	SOCP	IPM	SOCP(s)	IPM(s)	Total(s)
MEC-BH1 (t = 100)	38	8	6.01	5.78	11.79
MEC-BH2 (t = 100)	42	8	6.40	6.02	12.42

is given as an input to the optimization algorithm (the shaded portion of transients in Fig. 2). The black curves are transients obtained from the IPM algorithm applied to the optimization problem in (11). As the low-order $qd0$ model cannot capture all dynamics generated by the MEC model, the optimization algorithm will minimize the mismatch between the trajectories of the input MEC model and the extracted $qd0$ model.

The leakage inductance, L_{ls}, reported in [3], are obtained using the conventional zero-sequence test as documented in [34]. Alternatively, the leakage inductance value obtained here provides the best fit between the transients produced by MEC and *qd0* models. Fig. 4 compares the zero-sequence flux linkage, λ_{0s}, of MEC data against transients produced by two *qd0* models with two different sets of parameters. The waveform colored green (named '*qd0* [3]') corresponds to the *qd0* model with parameters taken from [3], while the waveform colored black (named '*qd0* optimal') corresponds to the *qd0* model with parameters from Table II. It is evident from Fig. 4 that the machine parameters obtained in this paper provide a better fit to the MEC data. Mean absolute percentage error (MAPE) [35] can be used to quantify the errors between the curves in Fig. 4. MAPE is defined as

$$\text{MAPE} = \frac{100\%}{T}\sum_{t=1}^{T}\left|\frac{Y_{\text{MEC}}(t) - Y(t)}{Y_{\text{MEC}}(t)}\right|, \tag{19}$$

where Y_{MEC} represents the transients from the MEC model and Y is the transients produced by the *qd0* models. The MAPEs for '*qd0* [3]' and '*qd0* optimal' compared to the MEC data for Fig. 4 are 40.04% and 37.42%, respectively.

Table IV provides the iteration counts and times required for both cone programming (CVX with the SDPT3 4.0 solver) and IPM (MIPS solver) methods. Note that the longer time horizon also increases the computation time needed to obtain the optimal

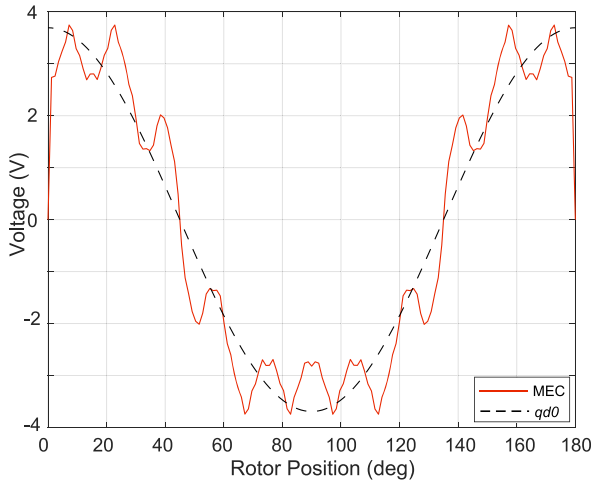

Fig. 5. Open-circuit operation of the static MEC model in [3] and the resulting $qd0$ model ($i_{fld} = 1$ A, $\omega_r = 1000$ RPM).

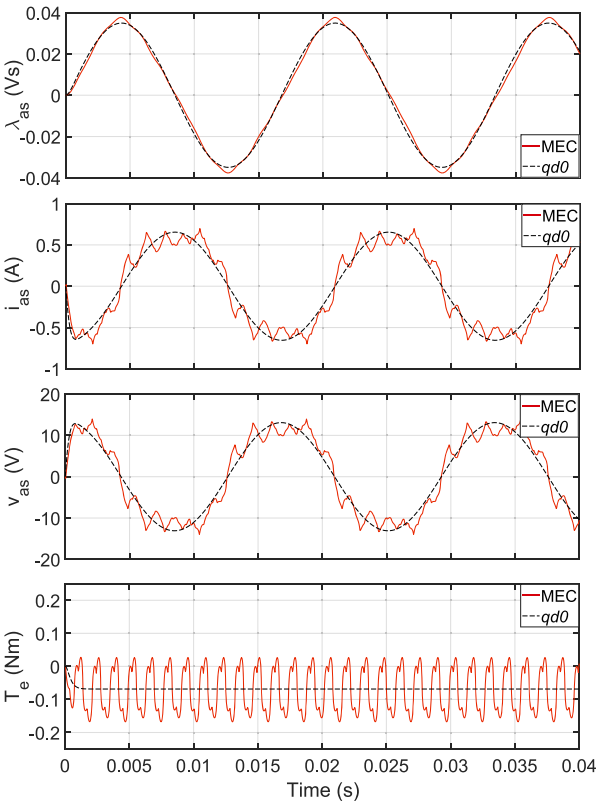

Fig. 6. Flux linkage, current, voltage, and electric torque for the extracted $qd0$ model compared against the MEC model, when connected to a balanced load ($i_{fld} = 1$ A, $\omega_r = 3600$ RPM, $R_{load} = 20\ \Omega$).

solution, as the number of unknown variables (and equality constraints) also increases.

D. MEC vs $qd0$ Model Comparison

The MEC model of the WRSM had been validated against a hardware prototype [3]. Herein, we reproduce Figure 10a of [3] to compare our $qd0$ model against the validated MEC model. The WRSM is run under an open circuit with $i_{fld} = 1$ A and $\omega_r = 1000$ RPM. Fig. 5 shows the phase-a voltage waveform for the extracted $qd0$ model, and that obtained by the static MEC model. The harmonic effects of the spatial distribution of stator slots are evident in the MEC model. The voltage waveform produced by both models are in agreement.

Next, the $qd0$ model and the dynamic MEC model are simulated with $i_{fld} = 1$ A, $\omega_r = 3600$ RPM, and a balanced load $R_{load} = 20\ \Omega$. The phase-a transients, as seen in Fig. 6, show that the resulting $qd0$ model mimic the essential dynamics of the MEC model. The physical time for a 5-cycle (83.3 ms) simulation run for the MEC and $qd0$ models are 0.8362 s and 0.0377 s, respectively. The $qd0$ model is more than 20 times faster than the dynamic MEC model.

VII. Summary

The macromodel of a 2 kW WRSM is successfully extracted from its dynamic MEC model. The parameter extraction process is formulated as an optimization problem; This problem is first covexified using a cone programming relaxation method and, then, the resulting solution is used to initialize the IPM solver. We have successfully extracted all the machine parameters within 4% accuracy with respect to the original MEC model; The leakage inductance, L_{ls}, was estimated within 10% accuracy. The extracted $qd0$ model is compared against MEC model, and exhibits acceptable fidelity with an appreciable gain in the simulation speed. Future work could include model extraction for a more general *qd0* model that accounts for spatial harmonics. This would be a compromise between the MEC model and the classical *qd0* model with constant inductance terms. We envision that adding any general form of *qd0* model would change the equality constraints of the optimization problem. To accommodate non-sinusoidal winding distributions, the flux linkage-current relation in (6) will include rotor-position-dependent inductance terms. Therefore, the equality constraints in (11c) will be updated to include expressions that are products of time-varying inductances and winding currents (instead of time-invariant inductances and currents). Given the circumferential motion of the rotor, additional equality constraints would be needed to address the periodicity of inductances.

Acknowledgment

We wish to thank the researchers at Purdue University for making their codes available online. We wish to thank Nuh Erdogan, from University College Cork, for fruitful comments.

References

[1] P. Krause, O. Wasynczuk, S. D. Sudhoff, and S. Pekarek, *Analysis of Electric Machinery and Drive Systems*. Hoboken, NJ, USA: Wiley, 2013.

[2] N. R. Tavana and V. Dinavahi, "A general framework for FPGA-based real-time emulation of electrical machines for HIL applications," *IEEE Trans. Ind. Electron.*, vol. 62, no. 4, pp. 2041–2053, Apr. 2015.

[3] M. L. Bash and S. Pekarek, "Analysis and validation of a population-based design of a wound-rotor synchronous machine," *IEEE Trans. Energy Convers.*, vol. 27, no. 3, pp. 603–614, Sep. 2012.

[4] M. L. Bash, J. M. Williams, and S. D. Pekarek, "Incorporating motion in mesh-based magnetic equivalent circuits," *IEEE Trans. Energy Convers.*, vol. 25, no. 2, pp. 329–338, Jun. 2010.

[5] M. L. Bash and S. D. Pekarek, "Modeling of salient-pole wound-rotor synchronous machines for population-based design," *IEEE Trans. Energy Convers.*, vol. 26, no. 2, pp. 381–392, Jun. 2011.

[6] R. Wang, S. Pekarek, M. L. Bash, A. Larson, and R. V. Maaren, "Incorporating dynamics in a mesh-based magnetic equivalent circuit model of synchronous machines," *IEEE Trans. Energy Convers.*, vol. 30, no. 3, pp. 821–832, Sep. 2015.
[7] H. W. Derbas, J. M. Williams, A. C. Koenig, and S. D. Pekarek, "A comparison of nodal-and mesh-based magnetic equivalent circuit models," *IEEE Trans. Energy Convers.*, vol. 24, no. 2, pp. 388–396, May 2009.
[8] G. Friedrich and A. Girardin, "Integrated starter generator," *IEEE Ind. Appl. Mag.*, vol. 15, no. 4, pp. 26–34, Jul. 2009.
[9] "Ieee guide for test procedures for synchronous machines part iacceptance and performance testing part ii-test procedures and parameter determination for dynamic analysis," *IEEE Std 115-2009*, vol., no., pp. 1–219, May 2010.
[10] M. Karrari and O. P. Malik, "Identification of physical parameters of a synchronous generator from online measurements," *IEEE Trans. Energy Convers.*, vol. 19, no. 2, pp. 407–415, Jun. 2004.
[11] E. Kyriakides, G. T. Heydt, and V. Vittal, "Online parameter estimation of round rotor synchronous generators including magnetic saturation," *IEEE Trans. Energy Convers.*, vol. 20, no. 3, pp. 529–537, Sep. 2005.
[12] J. J. S.-Gasca, C. J. Bridenbaugh, C. E. J. Bowler, and J. S. Edmonds, "Trajectory sensitivity based identification of synchronous generator and excitation system parameters," *IEEE Trans. Power Syst.*, vol. 3, no. 4, pp. 1814–1822, Nov. 1988.
[13] G. Valverde, E. Kyriakides, G. T. Heydt, and V. Terzija, "Nonlinear estimation of synchronous machine parameters using operating data," *IEEE Trans. Energy Convers.*, vol. 26, no. 3, pp. 831–839, Sep. 2011.
[14] T. Boileau, N. Leboeuf, B. Nahid-Mobarakeh, and F. M.-Tabar, "Online identification of pmsm parameters: Parameter identifiability and estimator comparative study," *IEEE Trans. Ind. Appl.*, vol. 47, no. 4, pp. 1944–1957, Jul. 2011.
[15] Ping Zhou, J. Gilmore, Z. Badics, and Z. J. Cendes, "Finite element analysis of induction motors based on computing detailed equivalent circuit parameters," *IEEE Trans. Magn.*, vol. 34, no. 5, pp. 3499–3502, Sep. 1998.
[16] A. Repo, P. Rasilo, A. Niemenmaa, and A. Arkkio, "Identification of electromagnetic torque model for induction machines with numerical magnetic field solution," *IEEE Trans. Magn.*, vol. 44, no. 6, pp. 1586–1589, Jun. 2008.
[17] O. Makela, A. Repo, and A. Arkkio, "Parameter estimation for synchronous machines using numerical pulse test within finite element analysis," in *Proc. 18th Int. Conf. Elect. Mach.*, 2008, pp. 1–5.
[18] S. Huang, Q. Wu, J. Wang, and H. Zhao, "A sufficient condition on convex relaxation of ac optimal power flow in distribution networks," *IEEE Trans. Power Syst.*, vol. 32, no. 2, pp. 1359–1368, Mar. 2017.
[19] J. Li, F. Liu, Z. Wang, S. H. Low, and S. Mei, "Optimal power flow in standalone dc microgrids," *IEEE Trans. Power Syst.*, vol. 33, no. 5, pp. 5496–5506, Sep. 2018.
[20] S. Bahrami, F. Therrien, V. W. S. Wong, and J. Jatskevich, "Semidefinite relaxation of optimal power flow for ac-dc grids," *IEEE Trans. Power Syst.*, vol. 32, no. 1, pp. 289–304, Jan. 2017.
[21] H. Kojooyan-Jafari, L. Monjo, F. Crcoles, and J. Pedra, "Parameter estimation of wound-rotor induction motors from transient measurements," *IEEE Trans. Energy Convers.*, vol. 29, no. 2, pp. 300–308, Jun. 2014.
[22] S. A. Odhano, P. Pescetto, H. A. A. Awan, M. Hinkkanen, G. Pellegrino, and R. Bojoi, "Parameter identification and self-commissioning in ac motor drives: A technology status review," *IEEE Trans. Power Electron.*, vol. 34, no. 4, pp. 3603–3614, Apr. 2019.
[23] V. H. Quintana, G. L. Torres, and J. M.-Palomo, "Interior-point methods and their applications to power systems: A classification of publications and software codes," *IEEE Trans. Power Syst.*, vol. 15, no. 1, pp. 170–176, Feb. 2000.
[24] P. Beyhaghi, D. Cavaglieri, and T. Bewley, "Delaunay-based derivative-free optimization via global surrogates, Part i: Linear constraints," *J. Global Optim.*, vol. 66, no. 3, pp. 331–382, 2016.
[25] M. Kojima, S. Mizuno, and A. Yoshise, *A Primal-Dual Interior Point Algorithm for Linear Programming*. New York, NY: Springer New York, 1989, pp. 29–47. [Online]. Available: https://doi.org/10.1007/978-1-4613-9617-8_2
[26] Y. Weng, Q. Li, R. Negi, and M. Ilic, "Semidefinite programming for power system state estimation," in *Proc. IEEE Power Energy Soc. General Meet.*, 2012, pp. 1–8.
[27] C. A. Rojas, J. I. Yuz, M. Aguirre, and J. Rodriguez, "A comparison of discrete-time models for model predictive control of induction motor drives," in *Proc. IEEE Int. Conf. Ind. Technol.*, 2015, pp. 568–573.
[28] R. Madani, M. Kheirandishfard, J. Lavaei, and A. Atamtürk, "Penalized conic relaxations for quadratically constrained quadratic programming," *Preprint*, Jun. 2019. [Online]. Available: http://www.uta.edu/faculty/madanir/penalty_paper.pdf
[29] R. H. Tütüncü, K. C. Toh, and M. J. Todd, "Solving semidefinite-quadratic-linear programs using SDPT3," *Math. Program.*, vol. 95, no. 2, pp. 189–217, Feb. 2003. [Online]. Available: https://doi.org/10.1007/s10107-002-0347-5
[30] MOSEK-Aps, *The MOSEK Optimization Toolbox for MATLAB Manual. Version 8.1.*, 2017. [Online]. Available: http://docs.mosek.com/8.1/toolbox/index.html
[31] M. Grant and S. Boyd, "CVX: Matlab software for disciplined convex programming, version 2.1," Mar. 2014. [Online]. Available: http://cvxr.com/cvx
[32] R. D. Zimmerman and H. Wang, "Matpower interior point solver MIPS 1.3 users manual," 2016.
[33] R. Wang, S. Pekarek, and M. Bash, "Alternative excitation strategies for a wound rotor synchronous machine drive," in *Proc. IEEE Energy Convers. Congr. Expo.*, 2012, pp. 2300–2307.
[34] H. Bai *et al.*, "Analytical derivation of a coupled-circuit model of a claw-pole alternator with concentrated stator windings," *IEEE Trans. Energy Convers.*, vol. 17, no. 1, pp. 32–38, Mar. 2002.
[35] R. J. Hyndman and A. B. Koehler, "Another look at measures of forecast accuracy," *Int. J. Forecasting*, vol. 22, no. 4, pp. 679–688, Oct.–Dec. 2006.

Ajay Pratap Yadav received the bachelor's degree from the Indian Institute of Technology Roorkee, Roorkee, India, in 2010 and the master's degree from the Indian Institute of Technology Kanpur, Kanpur, India, in 2014, both in electrical engineering. He is currently working toward the Ph.D. degree with The University of Texas at Arlington, Arlington, TX, USA. His research interests include electric machine modeling, system identification, optimization, and microgrids.

Tuncay Altun received the B.Sc. and M.Sc. degrees in electrical engineering from Yildiz Technical University, Istanbul, Turkey, in 2011 and 2014, respectively. He is currently working toward the Ph.D. degree with the University of Texas at Arlington, Arlington, TX, USA. His research interests include optimization and control for power systems applications, renewable/sustainable energy systems, microgrids, and HVdc transmission.

Ramtin Madani received the Ph.D. degree in electrical engineering from Columbia University, New York, NY, USA, in 2015. He is currently an Assistant Professor with the Department of Electrical Engineering, The University of Texas at Arlington, Arlington, TX, USA. His research interests include developing algorithms for optimization and control with applications in energy.

Ali Davoudi (Senior Member, IEEE) received the Ph.D. degree in electrical and computer engineering from the University of Illinois, Urbana-Champaign, IL, USA, in 2010. He is currently an Associate Professor with the Electrical Engineering Department, University of Texas, Arlington, TX, USA. He is an Associate Editor for the IEEE TRANSACTIONS ON POWER ELECTRONICS, the IEEE TRANSACTIONS ON TRANSPORTATION ELECTRIFICATION, the IEEE TRANSACTIONS ON ENERGY CONVERSION, and the IEEE POWER LETTERS. More recently, he has received the best paper award from 2015 IEEE International Symposium on Resilient Control Systems, 2014–2015 best paper award from the IEEE Transactions on Energy Conversion, 2016 Prize Paper Award from the IEEE Power and Energy Society, 2017 IEEE Richard M. Bass Outstanding Young Power Electronics Engineer Award, 2017–2018 best paper award from the IEEE Transactions on Energy Conversion, and 2019–2020 Faculty Fellow of Janet and Mike Greene Endowed Professorship.